Shipley, T.H., Ogawa, Y., Blum, P., and Bahr, J.M. (Eds.), 1997
Proceedings of the Ocean Drilling Program, Scientific Results, Vol. 156

14. ANALYSIS OF NATURAL GAMMA-RAY SPECTRA OBTAINED FROM SEDIMENT CORES WITH THE SHIPBOARD SCINTILLATION DETECTOR OF THE OCEAN DRILLING PROGRAM: EXAMPLE FROM LEG 156[1]

Peter Blum,[2] Alain Rabaute,[3] Pierre Gaudon,[4] and James F. Allan[2]

ABSTRACT

Natural gamma-ray (NGR) spectrometry allows estimation of the elemental concentrations of K, U, and Th, which can be used to help interpret sediment composition, provenance, and diagenesis. Spectral data obtained with the NGR multichannel device installed on the Ocean Drilling Program's multisensor track in 1993 are presented here for the first time. The spectra were divided into 16 energy intervals using a minima search algorithm that defined all peaks observed in 79 sample NGR spectra. The intervals were further subdivided into peak area and background area segments using a peak baseline algorithm, which allows optimal assessment of the usefulness of spectral segments to estimate elemental abundance. Linear regression with laboratory (X-ray diffraction, inductively coupled plasma-mass spectrometry, and instrumental neutron activation analyses) data was used to estimate elemental concentrations of K, U, and Th for each spectral segment. Conservative estimation errors for the best estimator spectral segments are 16%, 30%, and 20% for K, U, and Th, respectively. These errors also reflect analytical errors of the reference data, and the true estimation error may be significantly smaller. Our method suggests that the best K estimates (± 16%) are obtained using the peak area segment between 1335 and 1580 KeV. In our study, which uses 4-hr counting times, the best U and Th estimates are obtained using peak areas between 1695 and 1885 KeV and 550 and 700 KeV, respectively. If low counting times are used for routine core logging, however, regressions using the total counts of the entire spectrum yield more reliable U and Th estimates because of Poisson's law, with maximum total errors of about 35% and 23%, respectively. Spectral analysis using 2048-channel data has no advantage over 256-channel analyses, even with the extremely high counting times used for our study. The full character of natural gamma-ray spectra, as revealed by scintillation detectors, can be defined and measured in full detail with 16 energy intervals.

INTRODUCTION

Natural gamma radiation of geological formations has been measured by well logging for more than half a century (Serra, 1984). Prior to the 1980s, the total number of counts detected were mostly used as an indicator of "shaliness". In the 1970s, natural gamma-ray spectrometers were introduced to well-logging and airborne surveys (e.g., Grasty, 1975; Marett et al., 1976; Serra et al., 1980; Mathis et al., 1984). Natural gamma-ray (NGR) spectrometry allows estimation of elemental concentrations of potassium, uranium, and thorium through the gamma emission of their radioactive isotopes ^{40}K, the ^{238}U series, and the ^{232}Th series. These most important "primeval" natural gamma-ray emitters are at secular equilibrium with their parent elements (i.e., radiation at characteristic energies is constant with time; Adams and Gaspirini, 1970). The relative abundance of K, U, and Th estimated from well-logging data has been shown to help characterize clay type and abundance, depositional environment, and diagenetic processes in sediments (Serra et al., 1980; Serra, 1984, 1986).

Because NGR spectrometry provides rapid, continuous, and inexpensive lithological parameters in geological formation testing, we explored its adaptation to the routine continuous core logging of the Ocean Drilling Program (ODP). An NGR measurement device was installed by the ODP on the *JOIDES Resolution* in 1993 as part of the multisensor track (MST) for continuous core logging. General energy calibration, measurement, and correction procedures were introduced by Hoppie et al. (1994). The original intent for the instrument was to measure total counts to aid correlation of core and downhole geophysical data. However, the device is equipped with a 2048-channel multichannel analyzer and adequate software to allow spectral data acquisition. ODP had introduced the five-window spectral data acquisition used by its downhole measurement contractor, Schlumberger Services, to provide the scientists with a standard spectral data set, but no absolute calibration standards, model spectra, or estimation algorithms exist to estimate elemental concentrations.

NGR spectra of rocks and soils are composed of one emission peak of ^{40}K, more than a dozen emission peaks of the ^{238}U series (mainly ^{214}Bi), a similar number of ^{232}Th peaks (^{208}Tl, ^{228}Ac), and total background. Total background originates from two completely different sources. Zero-background is the combination of cosmic radiation, impurities in detector crystal, and contamination in the measurement system (e.g., soil deposits inside the lead shielding), and is unrelated to the composition of the measured material. It is determined separately and removed from core spectra before spectral analysis (Figs. 1, 2). What we will refer to as background from here on is produced by Compton scattering, photoelectric absorption, and pair production related to the abundance and distribution of primeval emitters, as well as by low-intensity, discrete emission peaks of U and Th, which disappear in the scatter.

Background, as well as limited detector efficiency degrade NGR spectra; only a few peaks are discernible as individual bell-shaped peak areas above background (Figs. 1, 2). In fact, the main, characteristic peaks above background for the three elements only comprise a few percent of the total counts of the entire spectrum. Using only these characteristic peaks may result in severe statistical counting errors at reasonable counting times. Therefore, the common method applied by commercial well-logging services and airborne surveys is to

[1]Shipley, T.H., Ogawa, Y., Blum, P., and Bahr, J.M. (Eds.), 1997. *Proc. ODP, Sci. Results*, 156: College Station, TX (Ocean Drilling Program).

[2]Ocean Drilling Program, Texas A&M University, College Station, TX 77845, U.S.A. peter_blum@odp.tamu.edu

[3]I.S.T.E.E.M, Laboratoire de Géochimie Isotopique, UMR 5567-CNRS, CC 066, Université Montpellier II, Place E. Bataillon, 34095 Montpellier Cedex 5, France.

[4]Ecole Nationale Superieure des Mines et Techniques Industrielles, Laboratoire P3MG, 16 Avenue de Clavieres, 30319 Ales Cedex, France.

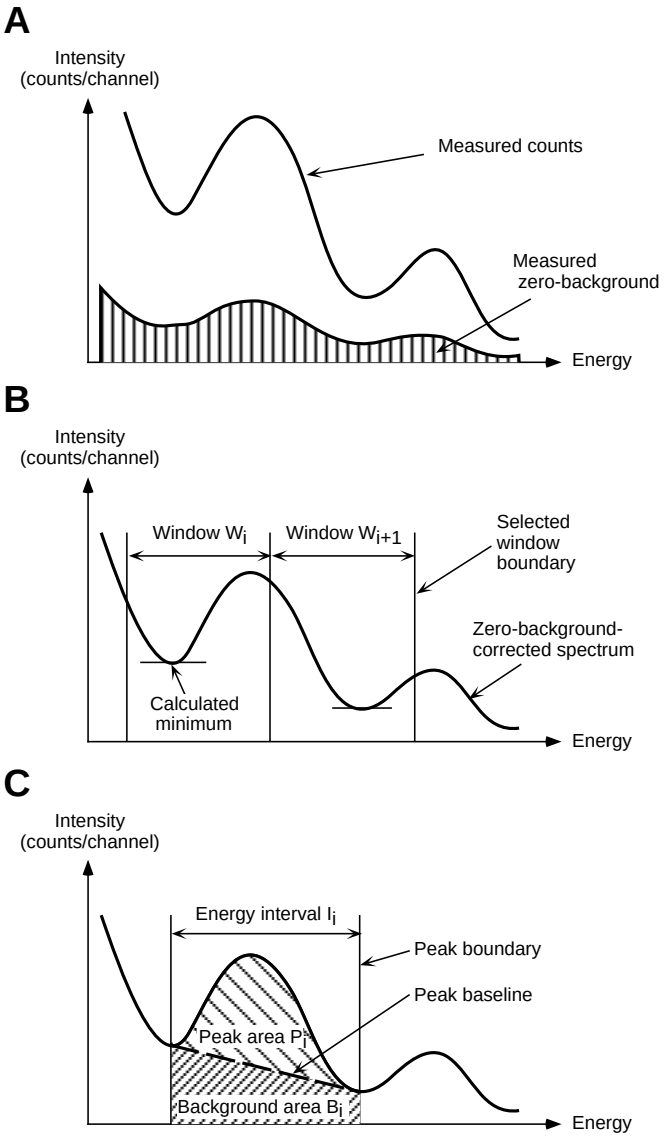

Figure 1. Schematic portion of a natural gamma-ray (NGR) spectrum illustrating the peak definition procedure. **A**. Zero-background, including cosmic radiation, impurities in sensor, and contamination in measurement area, is measured separately and subtracted from measured counts of sample spectra. **B**. In the zero-background–corrected spectrum, window boundaries are selected near energies of characteristic peaks identified from typical sample spectra. Minima are then calculated within each window for each sample spectrum. **C**. Peak baseline is defined by two adjacent minima and separates the integrated count area into peak area and background area.

include background in a simple three-standard calibration procedure under the assumptions that background in a given energy interval varies linearly with the abundance of the three elements, and that this relationship holds for all element distributions encountered. Elemental concentrations are then estimated using the method of weighted least squares, where the counts vector is the product of the sensitivity matrix and the concentration vector. The International Atomic Energy Agency (1976) suggests that K, U, and Th concentrations are calculated from counts in three discrete windows defined narrowly around the three main characteristic peaks (Fig. 2). The natural gamma-ray spectrometry (NGS) tool of Schlumberger Services uses five windows that form a continuous spectrum from 0.2 to 3.0 MeV (Serra et al., 1980) and has recently begun to acquire 256-channel spectra. Mathis et al. (1984) presented a window stripping and calibration study for the spectral gamma-ray (SGR) tool of Gearhart Services, which is based on 256 channels and provides either a routine three-window analysis or the raw spectra to the customer. For all these tools, elemental abundance is calculated using a sensitivity matrix obtained from segments of known concentrations of K, U, and Th in a calibration well.

Because the ODP system is not equipped with absolute calibration standards, we extracted core samples from the intervals measured with the ODP NGR device and determined reference concentrations in shore laboratories. We used linear regression to evaluate particular segments of the spectrum for their significance as elemental concentration estimators. The NGR spectra were measured for 4 hr to minimize counting errors, which was possible during Leg 156 because most of the time was expended for extensive downhole operations rather than for coring, allowing us to run an unusual number of dedicated NGR spectral measurements on idle instrumentation.

METHODS

Shipboard Natural Gamma-ray Measurements

During Leg 156, we acquired 79 natural gamma-ray spectra, 53 from Hole 948C and 26 from Hole 949B, using the shipboard NGR device and a commercial multichannel data acquisition program. The NGR system and its use are described in Hoppie et al. (1994). The NGR counts are detected and amplified by four 3×3 in, cylindrical, doped sodium iodide (NaI) scintillators and photomultiplier tubes that are arranged orthogonally around the measurement area and are collected by a 2048-channel analyzer. The energy spectrum was calibrated once at the beginning of the measurements, which extended over about four weeks, using K and Th. This calibration provides characteristic peaks at known energies for certain channel numbers. It does not quantify the spectra in terms of elemental concentrations, a task that would require about 0.5-m-long standards of ODP core geometry composed of homogenous mixtures of known elemental concentrations. We preferred K and Th over existing europium (Eu) calibration standards, because they provided the best possible linear calibration over the energy range that best represents the elements K, U, and Th. The calibration coefficients from the two-point linear relationship were applied to all spectra. Drift was negligible for our analysis, as discussed later. We counted split-core sections for 4 hr to minimize statistical counting errors. We could not measure unsplit cores, because our measurements would have severely delayed core splitting, description, and routine split-core measurements. We assume that the same results would have been obtained by measuring unsplit cores for 2 hr.

The zero-background was established by measuring air and pure-water spectra for 4 hr. In the first case, nothing was put into the system at all, whereas in the second case, we placed a core liner filled with pure water into the sensor's measurement area. The air and water spectra resemble each other closely, with no discernible difference in the high-energy half of the spectrum, and somewhat higher counts for the air measurements in the low-energy part of the spectrum. The slight difference is probably due to increased cosmic radiation in the air measurements. We chose to use the average spectrum of six water measurements, because they intuitively represent more closely the zero background during core measurements.

Elemental Analysis

Elemental analyses were conducted on 79 core samples that accurately represent the core intervals measured with the NGR. To eliminate potential sampling error caused by lithologic variation, we cut thin, 20-cm-long core samples centered at the core depth, which was in the center of the NGR measurement area. The core samples were dried, crushed, and split for X-ray fluorescence (XRF) analyses, inductively coupled plasma-mass spectrometer (ICP-MS) analysis, and

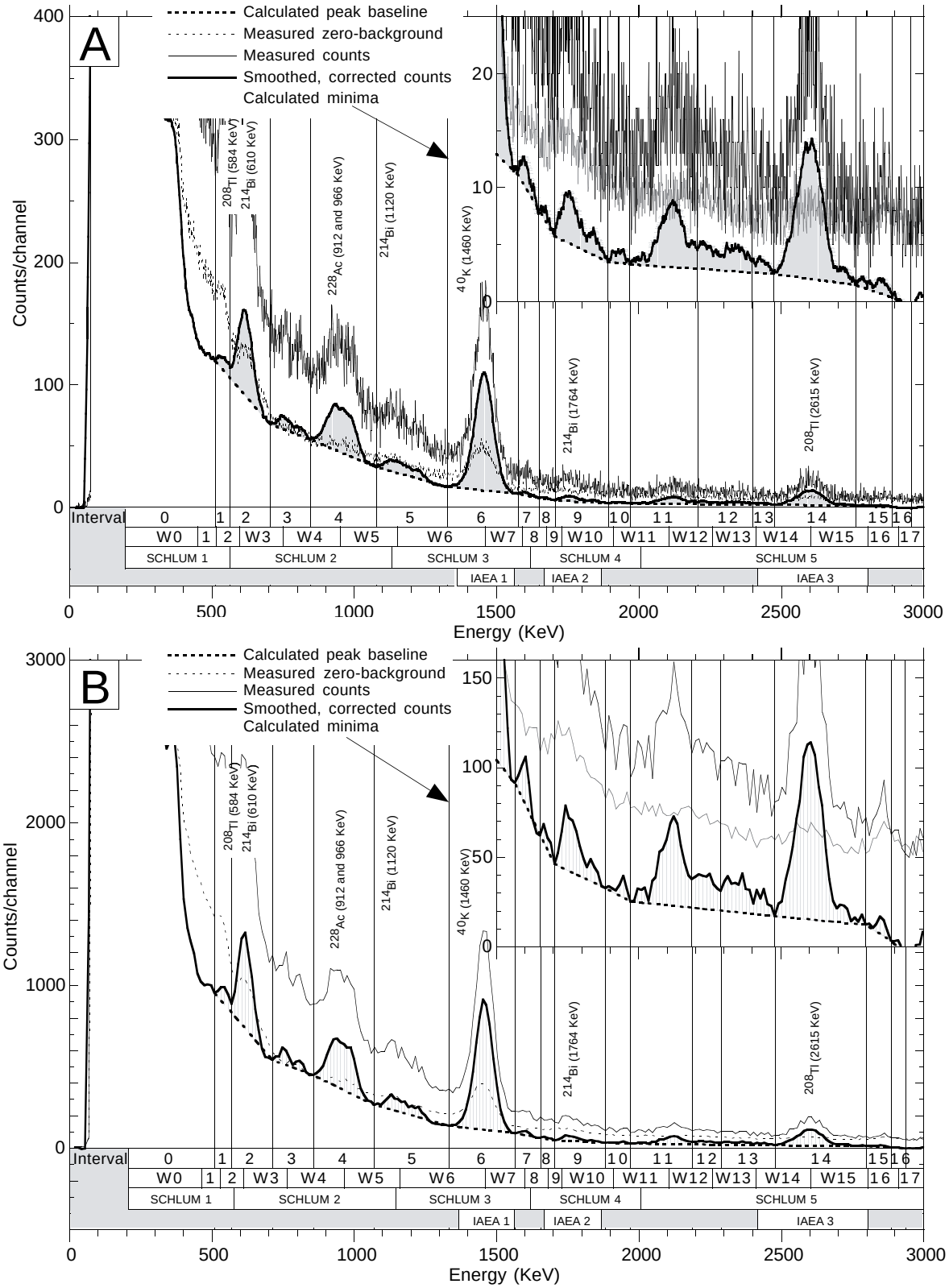

Figure 2. Example spectrum from Hole 948C sample. Insets are enlarged illustrations of the high-energy, low-count part of the spectrum, horizontal scale and positioning is the same as in main plot. Windows W0 to W17 are selected windows for minima calculations, and intervals 0 to 16 are defined by calculated minima (see Fig. 1). Shaded areas are peak areas. Schlum = Schlumberger Services. IAEA = International Atomic Energy Agency. **A.** 2048-channel data set. Bold line is 30-point smoothed, zero-background corrected. **B.** Same data as (**A**) with 256-channel resolution. Bold line is 3-point smoothed, zero-background corrected.

instrumental neutron activation analyses (INAA). Precision and accuracy are estimated from repeated standard measurements. Precision is expressed as the ratio of the first standard deviation of multiple measurements to their mean, in percentage, and represents the random (instrumental) measurement error. Accuracy is expressed as the ratio of the difference between measured mean and known (or accepted) value for the standard to the known value, in percentage (Table 1). This error may be random or biased, and originate either from the instrument or from the composition of the particular material measured. A conservative estimate of the total analytical error is the sum of errors due to precision and accuracy.

XRF analyses were carried out at the Ecole Nationale Superieure des Mines et Techniques Industrielles in Alès, France, on fusion beads using a lithium tetraborate + lanthanium oxide flux (0.750 mg sample per 6 g flux) to give the concentrations of the 10 major oxides: CaO, SiO_2, Al_2O_3, Fe_2O_3, K_2O, TiO_2, MgO, MnO, Na_2O, P_2O_5. We are only presenting the K_2O data in this study. Replicate analyses of rock standards show that precision of the major element data is 0.5%–2.5%, and accuracy is better than 1% for most elements, including K (Table 1).

ICP-MS was conducted at the Laboratoire de Géochimie Isotopique at the University of Montpellier II, France, for U and Th reference concentrations. One-hundred milligrams of powdered sample were dissolved in a 15-mL autoclavable Teflon threaded screw cap jar by repeated dissolution/evaporation with perchloric and fluorhydric acids in an oven. The samples were subsequently wetted with distilled water and dissolved in 1.5 mL of 65% HNO_3 solution. After complete dissolution, the sample was transferred into a 20.6 g sterile jar with a threaded screw cap, and the jar was filled with distilled water. A 10-ppb In-Bi internal calibration standard was added to 10 mL of this solution prior to ionization by the plasma source and determination of elemental concentrations by the mass spectrometer. Two samples could not be dissolved completely because of the presence of organic carbon and application of an unsuitable dissolution process. The data for these samples are omitted in our analyses. From the multiple standard measurements, precision was determined at 4% and 3%, and accuracy at 3% and 7% for U and Th, respectively.

INAA were conducted using a TRIGA reactor and counting facilities at the Center for Chemical Characterization at Texas A&M University. Fifty-milligram samples were irradiated for 14 hr and counted for 6 hr after decay periods of 9–12 and 40–43 days, using germanium detectors. Spectral analysis was made using a nuclear data program and was supplemented with manual U- and Th-series overlap and interference corrections. A total of 12 samples of the international AGV-1 standard were irradiated at multiple levels within the specimen holder during three runs, and were subsequently counted. Precision was 11% and 2% for U and Th, respectively. Mean AGV-1 values deviate from the accepted values of Gladney et al. (1992) by +9% and –1% for U and Th, respectively (Table 1).

All results are plotted as a function of depth in Figure 3. All U and Th results from ICP-MS and INAA are plotted in Figure 4, illustrating the degree of correlation between ICP-MS and INAA analyses. The fitted regression line is the reduced major axis (RMA; Till, 1974), which minimizes the product of the deviations in the x (ICP-MS) and y (INAA) directions, without regarding the results of one analyses as a function of the other. In effect, this minimizes the areas of the triangles formed by the data points and the fitted RMA, rather than the deviations in y (or x) direction.

Analytical data from Hole 948C specimens correlate relatively well, whereas Hole 949B data exhibit a considerable misfit. We therefore used only Hole 948C data for our NGR analysis. However, even in Hole 948C data, deviation from the RMA (or the diagonal) often exceeds the analytical precision range (error bars in Fig. 4), which effectively means that the total analytical error of one or the other (or both) data sets is considerably larger. Part of the difference is lack of accuracy, which we did not attempt to correct the reference for. Instead, we estimate a maximum uncertainty from the deviations between values from both measurement methods. Absolute deviations for each data pair (ΔU or ΔTh; Table 2) are expressed as ratios of the average values of the pair ($U_{AVERAGE}$ or $Th_{AVERAGE}$; Table 2). Mean and standard deviation of these ratios are listed in Table 2. For Hole 948C data, the uncertainty for U is at least 13% (mean of deviations). If the standard error of deviations is added, the uncertainty is 21%. For Th, the uncertainty is 7%, or up to 12% if standard error is added. These numbers are maximum error estimates that include systematic bias and variance of both analytical data sets. We chose to use only the data set with the smaller reported analytical error (i.e., ICP-MS data for U and INAA data for Th) and therefore the uncertainty of the reference data tends to be smaller. As an example, the systematic bias between U data from ICP-MS and INAA analyses, illustrated by the perfectly parallel offset of the RMA (Fig. 4A) and perhaps explained by the 9% relative overestimate of U concentrations by INAA (Table 2), is eliminated when using ICP-MS data only.

Analysis and Calibration of NGR Spectra

Our primary goal was to evaluate successive intervals of the spectra for their average information content in terms of elemental concentrations. The first part of the process comprised definition of potentially useful energy intervals and spectral segments (Figs. 1, 2) and evaluation of their properties from our sample spectra (averages, variances, ranges, etc.; Table 3). The second part of the process involved linear regression of the reference elemental concentrations with the counts of defined spectral segments. The following paragraphs describe the steps in more detail. All computations were performed with custom scripts and macros as well as available routines of a commercial plotting program. The data were processed for the full 2048-channel resolution (~1.5-KeV energy resolution) as well as a 256-channel resolution (~11.7-KeV energy resolution), which was simulated by binning the data before carrying out the computations.

1. *Zero-background correction.* An average zero-background spectrum that was obtained from six, 2048-channel water core measurements was subtracted from all 2048-channel sample spectra (Fig. 1A).

2. *Smoothing zero-background–corrected spectra.* After several trials with different smoothing parameters, 30-point smoothing was selected for the 2048-channel spectra, and 3-point smoothing for the 256-channel spectra. These values appeared to optimally remove spurious fluctuations thought to be the result of counting statistics, while preserving as much spectral information as possible.

3. *Finding minima for interval boundary definition.* Energy intervals associated with peaks are best defined by adjacent minima in the spectra. Minima are easily found by a computer if the spectral window for the search is defined. Visual examination of sample spectra revealed that fixed-window boundaries could be set near the ten most dominant peaks (Fig. 1B). A few iterations of calculating and plotting minima showed that some potentially useful peaks were not determined optimally. The window selection was therefore refined and resulted in 17 windows between 200 and 3000 KeV (first two columns in Table 2; W1 to W17 in bar at bottom of plots in Fig. 2). Some of these are relatively narrow to accurately target particular peak intervals (e.g., windows W7, W8, and W9 between main peaks of the K and U). The minima found within these windows defined 16 energy intervals. The additional interval 0 spans between the lowermost, fixed limit at 200 KeV and the first calculated minimum.

4. *Calculating peak baseline.* The peak baseline separates the energy interval into two segments, the peak area and the background area (Fig. 1C). The peak baseline between adjacent minima is defined by the linear equation

$$y = A + Bx, \quad (1)$$

where y is the number of background counts at energy x, and the coefficients A and B define the baseline in each energy interval.

Based on the assumption that the combined baseline curve of adjacent intervals should be rather smooth and continuous, we decided

Table 1. Laboratory analyses of potassium, uranium, and thorium.

Core, section, interval (cm)	Depth (mbsf)	XRF K_2O (%)	ICP-MS U (ppm)	ICP-MS Th (ppm)	INAA U (ppm)	INAA Th (ppm)
156-948C-						
2X-1, 65–85	421.45	2.87	1.87	11.61	1.99	12.21
2X-3, 65–85	424.45	2.20	1.58	7.79	1.59	8.29
2X-5, 65–85	427.45	2.84	2.06	11.85	2.74	12.69
3X-1, 65–85	431.15	2.38	1.71	9.02	1.97	10.52
3X-3, 65–85	434.15	2.40	1.89	8.97	2.16	9.23
3X-5, 65–85	437.15	2.19	?	?	2.41	10.74
4X-1, 65–85	440.75	2.49	?	?	1.96	12.18
4X-3, 65–85	443.75	2.11	1.28	9.56	1.63	9.70
4X-5, 65–85	446.75	2.34	1.54	11.45	1.72	12.21
5X-1, 65–85	450.45	2.20	1.49	9.53	1.62	10.60
5X-3, 65–85	453.45	1.86	1.29	8.86	1.46	8.88
5X-5, 65–85	456.45	1.62	1.35	7.55	1.43	8.11
6X-1, 65–85	460.05	1.97	1.44	8.40	1.69	8.92
6X-3, 65–85	463.05	2.00	1.60	9.48	1.93	10.30
7X-1, 65–85	469.65	1.63	1.03	6.20	1.36	6.66
7X-3, 65–85	472.65	2.00	1.18	7.50	1.34	8.76
7X-5, 65–85	475.65	1.55	0.95	5.29	1.33	6.17
8X-1, 65–85	479.35	1.74	1.38	7.83	1.47	8.81
8X-3, 65–85	482.35	1.15	1.10	4.65	1.12	4.84
8X-5, 65–85	485.35	1.53	1.22	6.91	1.34	7.43
9X-1, 65–85	489.05	0.81	1.00	3.88	0.92	4.00
9X-3, 65–85	492.05	1.13	1.68	5.07	2.06	5.14
9X-5, 65–85	495.05	1.39	1.46	8.00	1.90	9.20
10X-1, 65–85	498.75	1.33	1.61	8.41	1.81	8.87
10X-3, 65–85	501.75	1.55	1.80	10.40	2.33	11.25
10X-5, 65–85	504.15	1.47	1.76	10.28	2.19	11.30
11X-1, 65–85	508.35	1.23	1.39	9.90	1.53	10.43
11X-3, 65–85	511.35	1.80	2.24	17.71	2.42	17.37
11X-5, 93–113	514.63	2.12	2.14	14.64	2.22	15.37
12X-1, 65–85	518.05	2.37	2.01	14.60	2.84	14.80
12X-3, 65–85	521.05	2.20	2.67	14.87	2.67	13.89
12X-5, 65–85	524.05	2.74	4.72	12.88	6.13	13.20
13X-1, 65–85	527.45	2.59	2.89	13.89	3.28	14.28
13X-3, 95–115	530.75	1.46	5.69	13.82	4.83	11.26
13X-5, 65–85	533.45	2.50	3.12	13.89	3.29	13.49
14X-1, 65–85	536.75	2.66	2.56	14.90	2.83	15.60
14X-3, 65–85	539.75	2.88	2.12	16.62	2.47	17.62
14X-5, 65–85	542.75	2.46	3.43	14.28	3.84	15.10
15X-1, 65–85	546.05	1.66	1.79	14.63	2.06	15.48
15X-3, 65–85	549.05	1.93	3.35	15.78	3.42	14.04
15X-5, 65–85	552.05	2.54	1.47	14.29	1.71	14.76
16X-1, 65–85	555.45	2.30	2.10	15.23	2.22	16.70
16X-3, 65–85	558.45	1.88	1.59	16.34	1.81	16.13
16X-5, 65–85	561.45	1.17	3.27	9.39	3.70	9.89
17X-1, 65–85	564.75	3.24	2.33	16.91	2.46	18.01
17X-3, 65–85	567.75	2.98	2.11	14.85	2.35	15.60
17X-5, 65–85	570.75	2.49	3.06	15.00	3.32	13.85
18X-1, 65–85	573.95	1.94	4.69	18.63	4.35	15.20
18X-3, 65–85	576.95	1.49	2.12	12.31	2.03	12.38
18X-5, 65–85	579.95	2.71	2.45	16.45	2.86	17.36
19X-1, 65–85	583.45	1.96	1.63	14.01	1.80	14.88
19X-3, 65–85	586.45	3.02	2.81	17.19	3.34	16.01
19X-5, 65–85	589.45	2.03	2.36	13.62	2.50	14.17
156-949B-						
2X-4, 65–85	259.05	2.57	1.58	11.48	1.71	12.08
3X-1, 65–85	264.25	1.82	1.51	3.41	2.24	8.03
3X-3, 65–85	267.25	1.98	1.42	8.83	1.51	9.85
3X-6, 75–95	271.85	1.99	1.35	8.01	1.79	8.38
4X-1, 55–75	273.75	1.99	1.36	8.23	1.37	8.51
5X-1, 65–85	283.55	1.91	1.19	7.31	1.46	8.09
5X-3, 65–85	286.55	1.91	1.59	10.69	1.59	11.32
5X-5, 65–85	289.55	1.79	1.24	7.82	1.19	8.86
7X-1, 65–85	302.85	1.65	2.26	16.53	1.51	10.89
7X-3, 65–85	305.85	2.48	2.07	15.14	1.79	12.39
7X-5, 65–85	308.85	1.93	1.70	12.34	1.63	11.49
13X-2, 65–85	352.45	2.35	1.64	11.46	1.48	11.47
14X-2, 90–110	357.40	2.18	2.17	15.41	1.86	10.26
14X-3, 70–90	358.70	1.96	3.08	8.19	3.36	8.76
14X-5, 60–80	361.60	2.21	1.58	10.09	1.80	10.58
15X-2, 55–75	362.05	2.24	1.55	10.27	1.50	11.21
15X-4, 65–85	365.15	2.28	1.53	8.16	1.42	10.09
15X-6, 80–100	368.30	2.30	1.42	8.56	1.93	9.40
19X-1, 100–120	399.90	1.55	1.59	9.85	1.68	10.88
19X-4, 15–35	403.05	1.44	2.20	8.94	2.53	9.50
22X-1, 65–85	428.15	2.17	1.92	3.89	2.32	16.08
22X-3, 55–75	431.05	2.22	4.50	23.00	3.87	15.87
22X-5, 65–85	434.15	2.39	4.28	14.49	4.68	13.19
25H-1, 56–66	459.06	3.12	2.76	19.79	2.11	14.89
25H-1, 82–102	459.32	2.98	3.91	18.85	3.43	16.12
25H-2, 53–73	460.53	0.73	9.01	18.24	6.35	12.25
Analytical precision:		±2%	±4%	±3%	±11%	±2%
Accuracy:		1%	3%	7%	+9%	–1%

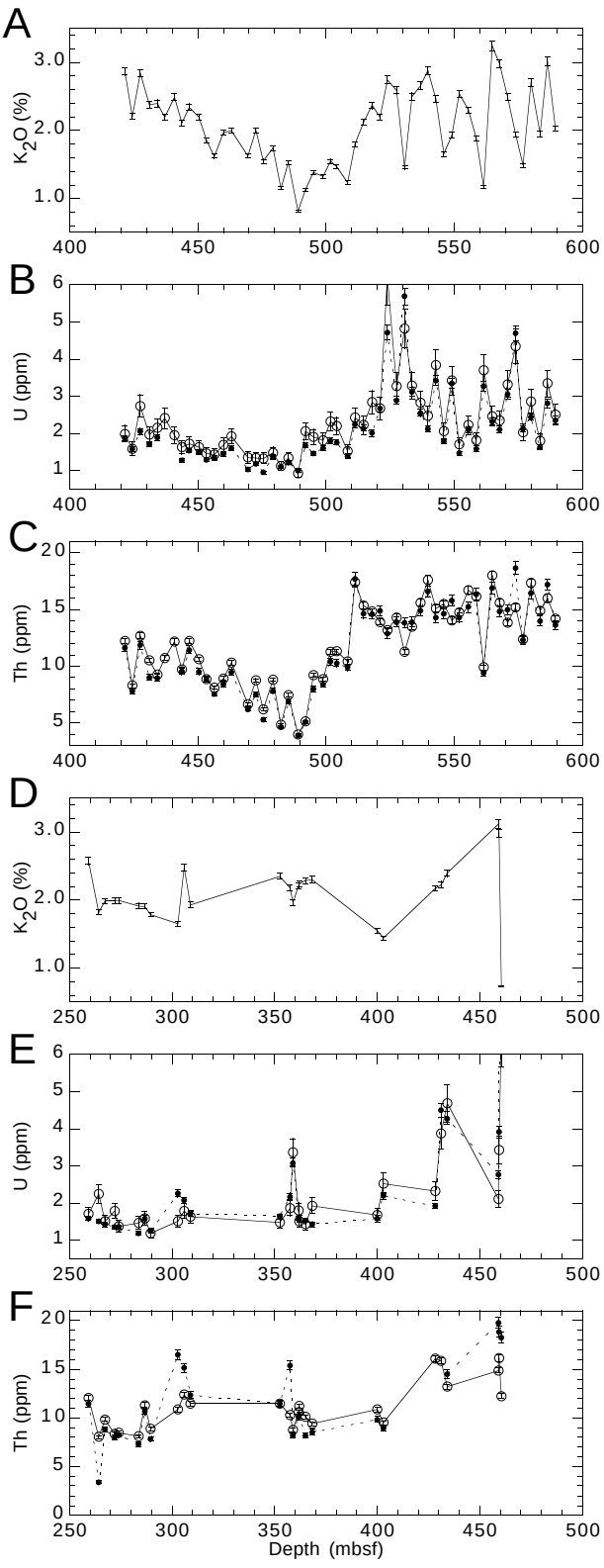

Figure 3. Depth plots of K, U, and Th reference concentrations. **A–C:** Hole 948C. **D–F:** Hole 949B. K concentrations are from XRF analyses. U and Th concentrations are from ICP-MS (solid circles) and INAA (open circles) analyses. Error bars indicate analytical precision.

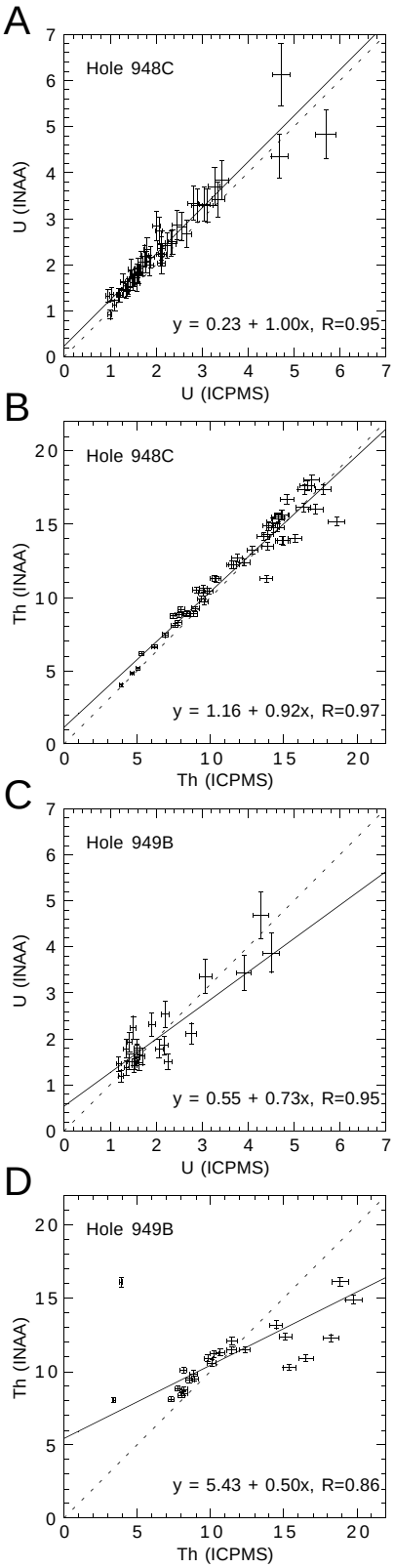

Figure 4. Comparison of ICP-MS and INAA analyses for U and Th from Holes 948C and 949B. Solid line is reduced major axis, a regression line which minimizes triangle areas with data points instead of the offsets parallel to one of the plot axes. Dashed lines are diagonals. Error bars are analytical precision. Hole 949B data indicate considerable analytical problems and were therefore not used for the NGR analyses. **A–B:** Hole 948C. **C–D:** Hole 949B.

to calculate common peak baselines for energy intervals 1 and 2, 7 and 8, and 11 through 13. Calculating individual baselines for these intervals would often have resulted in baselines of vastly different slopes compared to adjacent baselines, as well as unrealistically high ranges of average peak area counts.

5. *Integrating peak area and background area.* For each energy interval comprising k channels with zero-background–corrected counts c_i and baseline counts b_i, peak area P and background area B were computed as

$$B = \sum_{i=1}^{k} b_i$$

$$P = \sum_{i=1}^{k} (c_i - b_i). \quad (2)$$

Average values for 53 samples from Hole 948C are listed in Table 3. We did not calculate a peak baseline for interval 0 due to the overwhelming dominance of scatter counts in that low-energy part of the spectrum. Interval 0 is considered to be entirely background.

6. *Linear regression.* For each spectral segment (peak area or background area), least squares linear regressions between reference elemental concentrations x and integrated counts S (B or P areas) were performed using data from the 53 specimens of Hole 948C. This yielded linear coefficients M1 and M2 for each segment and each element, where:

$$S = M1 + M2x. \quad (3)$$

Pearson correlation coefficients R are listed in Table 4. A regression was also computed using the total counts (TC) from the entire spectrum (all peaks and background from ~0 to 2.9 MeV; first row in Table 4). Correlation with TC is the threshold of usefulness: if R for a particular peak or background segment is larger than the coefficient from the TC regression, that particular segment is a useful estimator of elemental abundance.

7. *Estimation errors*. The regression coefficients M1 and M2 were used to estimate elemental abundance x' for each of the 53 samples in each spectral segment, where:

$$x' = \frac{S - M1}{M2}. \quad (4)$$

Regressions using total counts and the main peak area of each element are shown in Figure 5, illustrating the maximum improvement possible over total counts estimates. Estimated concentrations x' were compared with their corresponding laboratory value x (XRF data for K, ICP-MS data for U, and INAA data for Th), and percent deviation, %Δ, was calculated for each specimen and each spectral segment:

$$\%\Delta = \frac{x - x'}{x} 100\%. \quad (5)$$

For each spectral segment, the mean and standard deviation of all %Δ from 53 specimens was calculated. We consider the sums of means and standard deviations, as illustrated in Figure 6, to represent the most conservative estimation errors for the segments. If the error for a particular segment is less than the error for the total counts estimate, the segment is considered a useful estimator.

DISCUSSION

General Characteristics of Sample Spectra

Our procedure of calculating energy intervals of all discernible peaks in the spectra allowed us to evaluate the average characteristics of many sample spectra (Table 3). Even though calculation of energy interval boundaries is based on an initial, visual identification of peaks, the general validity of the calculated interval boundaries, at least for our 70 sample spectra, is confirmed by consistent and low standard deviations around mean energies (2–33 KeV; see Table 3). Interval boundaries of the high-energy part of the spectra have higher standard deviations (20–33 KeV) than those from the low-energy part (2–16 KeV) due to higher statistical error associated with lower counts (Fig. 2; Table 3).

The mean from all 53 specimens (Hole 948C) of the peak maximum energy in intervals 6 and 14 (main peaks of K and Th, respectively; Table 3) are used to estimate the energy calibration drift during our shipboard measurements. The well-known energies of these calibration peaks are 1.46 and 2.62 MeV, and our corresponding mean values are 1.457 ± 0.004 and 2.594±0.013. Maximum drift of 0.03 MeV for the Th peak does not alter our spectral analyses significantly since energy intervals are typically 0.1–0.3 MeV wide (Fig. 2), and drift can be assumed to be linear.

We have identified good, fair, and poor peaks based on regular bell shape, consistent appearance throughout all sample spectra, and the relative range of integrated count areas (Table 3). Mean counts for peak and background areas from all 53 samples represent the average contribution of a spectral segment to the total counts, and the relative range is the range of counts for each segment expressed in percent of the mean (Table 3). Well-defined peak areas show only slightly higher relative range values than the reference concentrations from Hole 948C samples (120% for K and Th; 220% for U), suggesting a significant correlation. Most of the dominant gamma-ray emitter peaks are well defined (intervals 2, 4, 5, 6, and 14; see Fig. 2). In addition, the peak of interval 11 is also well defined. The main U peak (interval 9) is only fairly well defined due to low average counts. Most of the other peaks (intervals 1, 3, 7, 8, 10, 11, 12, 13, 15, and 16) have relative count ranges of more than 220%, which suggests poor correlation with reference data. Furthermore, we note that relative ranges of background areas are less than 170% for all low-energy intervals (B0 through B6), and mostly more than 200% for all high-energy intervals (Table 2). This suggests that the high-count rate, low-energy backgrounds may correlate equally well with the reference data as the well-defined peak areas.

Spectral Segments as Estimators of Elemental Abundance

The relationships between count segments and reference concentrations are explored using the correlation coefficient R, which is derived from linear regressions of reference concentrations with peak and background count areas (Table 4; Figs. 5, 6). Regressions of total counts with reference concentrations provide the threshold values, which are 0.67, 0.64, and 0.88 for K, U, and Th, respectively. Larger R-values are printed in boldface in Table 4 and indicate potentially useful estimator segments. Lower values of R indicate segments that do not provide better estimates for a particular element than the total spectrum. Similarly, potentially useful estimator segments are indicated by estimation errors smaller than those for total counts, which are 30%, 32%, and 20% for K, U, and Th, respectively (Fig. 6, Table 4). Both R-values and estimation error values identify the same spectral segments as potentially useful estimators, with one exception, as discussed below (P14 for K). For K these are, in the order of descending values of R, peak area P6 and background areas B5, B4, and B3; for U they are P9, P2, B9, B6, and B0, and for Th they are P4 and P14.

For K, P6 is clearly the best estimator (Fig. 6A). The interval is between 1335 and 1580 KeV which is practically the same as the interval proposed by the IAEA (1.37–1.57 MeV). Our results show, however, that stripping the background area, B6, significantly improves the estimate.

The relatively good K estimates by the three background segments of subsequently lower energy (B5 through B3) may reflect the effect of Compton scattering due to ^{40}K radiation. However, it may

Table 2. Summary of uncertainties associated with laboratory analyses of Uranium and Thorium.

Calculated for each data pair	Hole 948C Mean	Hole 948C SD	Hole 949B Mean	Hole 949B SD
Uranium				
$U_{AVERAGE} = \frac{U_{ICPMS} + U_{INAA}}{2}$	2.22		2.28	
$\Delta U = \sqrt{(U_{ICPMS} - U_{INAA})^2}$	0.29	0.25	0.39	0.52
$Relative\ deviations = \frac{\Delta U}{U_{AVERAGE}}$	13%	8%	15%	12%
Thorium				
$Th_{AVERAGE} = \frac{Th_{ICPMS} + Th_{INAA}}{2}$	11.81		11.34	
$\Delta Th = \sqrt{(Th_{ICPMS} - Th_{INAA})^2}$	0.78	0.61	2.47	2.89
$Relative\ deviations = \frac{\Delta Th}{Th_{AVERAGE}}$	7%	5%	22%	27%

Note: SD = standard deviation

also be an effect of the relatively good correlation between K and Th abundance in our samples (compare Figs. 3A and 3C), which causes our K regression to respond to good estimators of Th. Segment P14, which has a lower estimation error than total counts for K (Fig. 6A), shows this effect very clearly. We know *a priori* that it is impossible for K emissions to occur at such a high energy and that this interval is an excellent estimator of Th. Similarly, Th estimation errors in Figure 6C show a suspicious valley for P6, the main estimator of K. This statistical effect cannot be avoided unless downhole variations of the three elemental concentrations are completely uncorrelated, which is rarely the case in a natural system. Correlation between the three components does affect our R and estimation error values to some degree, but it is unlikely to alter the main results of our spectral analysis.

Our data suggest that only peak area P6 should be used for K estimates. This may be practical in most cases, because this is the largest peak area in the spectrum, and sufficient counts should accumulate to determine K concentration.

For U and Th, use of multiple segments for estimating elemental abundance may be advised. For uranium, P2 (^{214}Bi emissions at 610 KeV) and B9 (^{214}Bi emissions in background at 1720 KeV) are almost equally efficient estimators as the main peak area P9, and B6 and B0 are very good estimators too. For Th the best estimator in our study is P4 (^{228}Ac emissions) and not the well-known main P14 (^{208}Tl emissions), which ranks second. Several low-energy intervals show generally good correlation with Th abundance due to numerous emitters as well as their scatter products, which disappear into the background. Using them, however, would clearly degrade the estimate.

Our results show that for U and Th, total errors are not significantly reduced by using the best estimator segments (P9 and P4, respectively) rather than total counts. The spectra's worst estimators, indicated by large errors in Figure 6 (e.g., P7, P8, P10, and P13), are very low count intervals, and their weight is negligible in the total spectrum. Relatively good additional estimators (e.g., B2 through B6 for Th) are caused by numerous emission peaks of lower energy, which contribute significantly to the background. This is not the case for K, and that is why a background-free spectral component provides the best concentration estimate for potassium.

Errors of concentration estimates from NGR measurements are rarely reported, and if numbers are presented they are rarely explained. This is unfortunate because results from different methods, instruments, or companies cannot be compared (Hurst, 1990). Our sum of mean (equivalent to the accuracy of the estimate) and standard deviations (equivalent to the precision of the estimate) of percent deviations, as explained earlier, is a conservative error assessment for our 53 sample spectra. Using spectral segments P6, P9, and P4, these total estimation errors, which also reflect analytical errors of the reference data obtained in the laboratory, amount to 16%, 30% and 20% for K, U, and Th, respectively.

Counting Time and Precision

If our calculated estimation errors would apply to routine core logging, spectral gamma-ray measurements would be quite useful for estimating K, U, and Th abundance. Unfortunately, reduced counting times increase statistical counting errors, or noise, due to the fact that gamma-ray emissions are random events. Precision of NGR measurements is proportional to the number of counts according to Poisson's law, or:

$$P = \frac{0.67\sqrt{N}}{N}100\,, \qquad (6)$$

where P is the probable error in percent, and N is the number of counts. Typical routine measurements of 20 s on full-core sections are 360× shorter than our 4 hr measurements on split-core sections.

Counting time is usually limited for practical purposes. In well logging, the constraint is logging speed, which must be commercially justifiable and compatible with other, simultaneous measurements. In the case of continuous coring carried out by ODP, the time available to log a unit length of core is mostly dictated by the rate of core recovery. Leg 156 was a special case where most ship time was consumed by downhole operations, which left us plenty of time to measure the relatively few cores on idle instrumentation. On high-recovery legs, however, cores must usually be processed at a rate of ~10 m/ hr. This constrains practical NGR counting times to 20–40 s at depth intervals of 10–20 cm. If a NGR core logging device existed at a core repository, these constraints would not exist, and high-precision NGR spectra would be very affordable.

Table 5 demonstrates how the negligible counting errors for our 4-hr counting times, which are smaller than the laboratory analytical errors, increase dramatically for 20-s counting times. All potentially

Table 3. Summary of spectral segment calculations from 53 spectra from Hole 948C.

	Selected window boundaries (KeV)	Calculated interval boundaries		Some standard interval boundaries			Peak max. energy		Peak area		Background area		
		Mean (KeV)	SD (KeV)	IAEA (KeV)	Schlum (KeV)		Mean (KeV)	SD (KeV)	Mean (counts)	Range (% of mean)	Mean (counts)	Range (% of mean)	Peak definition
Window 0	200	N/A	N/A		200	Interval 0	251;259	7;0	N/A	N/A	103,823;98,721	139;139	N/A
Window 1	520	510;504	12;11		500	Interval 1	522;520	10;15	213;308	353;300	5,977;7,129	158;152	Poor
Window 2	600	566;569	3;2			Interval 2	616;617	3;3	3,214;3,299	149;152	12,195;11,990	148;130	Good
Window 3	750	714;714	13;12			Interval 3	752;751	10;9	596;617	225;199	8,548;8,505	149;178	Fair
Window 4	950	859;858	8;10			Interval 4	937;938	5;5	3,451;3,482	146;142	8,952;8,999	154;146	Good
Window 5	1150	1,065;1,063	14;14		1,100	Interval 5	1,128;1,126	15;14	1,377;1,407	149;154	6,653;6,795	166;166	Good
Window 6	1450	1,333;1,333	13;16	1,370		Interval 6	1,457;1,456	3;5	7,792;7,798	138;138	3,013;2,982	146;150	Good
Window 7	1590	1,574;1,570	10;9	1,570	1,590	Interval 7	1,596;1,597	12;12	76;81	296;309	744;768	227;202	Poor
Window 8	1670	1,662;1,658	14;15			Interval 8	1,671;1,669	7;8	7;6	2,294;2,968	199;228	293;270	Poor
Window 9	1720	1,694;1,694	13;13	1,660		Interval 9	1,756;1,760	16;17	296;295	246;130	987;971	189;168	Fair
Window 10	1900	1,887;1,879	14;21	1,860		Interval 10	1,912;1,911	20;28	42;45	346;165	337;375	243;270	Poor
Window 11	2100	1,988;1,987	34;39		2,000	Interval 11	2,126;2,124	22;18	544;503	140;136	665;628	247;212	Good
Window 12	2250	2,229;2,217	19;24			Interval 12	2,266;2,264	29;33	248;274	189;224	349;360	227;296	Fair
Window 13	2400	2,381;2,369	27;34			Interval 13	2,403;2,399	18;25	45;63	290;320	141;171	242;326	Poor
Window 14	2600	2,452;2,454	25;23	2,410		Interval 14	2,594;2,594	12;13	1,131;1,128	150;144	476;480	194;214	Good
Window 15	2800	2,775;2,777	20;20	2,810		Interval 15	2,812;2,810	24;18	43;38	221;274	68;68	370;286	Poor
Window 16	2900	2,873;2,867	28;21			Interval 16	2,903;2,897	25;22	31;30	434;130	32;38	594;490	Poor
Window 17	3000	2,857;2,950	33;33		3,000								

Notes: Data from 2048- and 256-channel analyses are given in each column as uvw;xyz respectively. Counting time was 4 hr. IAEA = International Atomic Energy Agency. Schlum = Schlumberger Services. SD = standard deviation. Window 0 to Window 17 were defined to constrain calculation of interval boundaries. N/A = not applicable.

Table 4. Correlation coefficients R used to evaluate potentially useful estimator segments.

		K		U		Th	
Interval		Peak	Bkg.	Peak	Bkg.	Peak	Bkg.
Total counts			*0.670*		*0.639*		*0.882*
Interval	0	-	0.643	-	**0.657**	-	0.877
Interval	1	–0.003	0.592	–0.071	0.422	0.073	0.758
Interval	2	0.470	0.650	**0.758**	0.614	0.816	0.847
Interval	3	0.463	**0.673**	0.492	0.629	0.786	0.863
Interval	4	0.617	**0.720**	0.517	0.583	**0.925**	0.857
Interval	5	0.645	**0.749**	0.564	0.605	0.691	0.850
Interval	6	**0.889**	0.654	0.421	**0.662**	0.789	0.860
Interval	7	0.259	0.551	–0.061	0.576	0.319	0.814
Interval	8	–0.090	0.272	–0.247	0.231	–0.253	0.448
Interval	9	0.257	0.485	**0.782**	**0.742**	0.492	0.772
Interval	10	–0.110	0.456	–0.195	0.499	–0.112	0.703
Interval	11	0.518	0.571	0.474	0.580	0.726	0.821
Interval	12	0.340	0.441	0.423	0.607	0.662	0.824
Interval	13	0.231	0.398	–0.095	0.344	–0.012	0.537
Interval	14	0.664	0.521	0.495	0.594	**0.899**	0.845
Interval	15	–0.229	0.275	–0.105	0.294	–0.137	0.591
Interval	16	0.185	0.401	0.394	0.366	0.253	0.589

Notes: R values are derived from linear regressions between K, U, and Th reference concentrations and count rates in each peak and background spectral segment, obtained from 53 specimens from Hole 948C. K, U, and Th reference data are from XRF, ICPMS, and INAA analyses, respectively. Peak and background values that are larger than total counts values shown in top row (potentially useful estimators, printed in italic face) are printed in bold face. Interval = calculated energy interval. Peak = integrated peak area of an interval. Bkg. = integrated background area of an interval.

useful spectral segments for K, U, and Th are listed in the order of decreasing significance, with their count values and estimation errors. Next, we have computed cumulative count values by adding the counts of the subsequent segment for each element, cumulative estimation errors weighted by the relative number of counts, and counting errors calculated according to Equation 6 and using the cumulative counts. All computations are made for the original 4-hr (14,400 s) counts on split cores and for hypothetical 20-s counts on full cores. The results may have implications for the choice of spectral segments to be used for elemental estimates when counting times are low. For K, using the main peak area P6 is still the best solution, because estimation errors increase faster than counting errors decrease when adding background areas B5, B4, and B3. The reason is the single emission energy of ^{40}K, which makes peak area P6 an overwhelmingly good estimator. For U and Th, however, adding certain spectral segments decreases the counting error dramatically, whereas the estimation error is not increased significantly. The reason is that multiple emitters across the spectrum contribute to the background, whereas relatively few counts accumulate in the best estimator segments.

Effect of Energy Resolution

All 79 sample spectra were analyzed for 2048-channel (~1.5 KeV) and a simulated 256-channel (~11.7 KeV) energy resolution. Table 3 shows that calculated interval boundaries as well as peak maxima energies differ by 2–12 KeV between the 2048- and 256-channel data sets. Standard deviations for these parameters from 53 sample spectra range from 2 to 39 KeV. They are very similar for higher and lower resolution data sets for a given energy interval. Variations in peak parameters related to the difference in energy resolution are therefore less significant than variations due to variance in the sample spectra. Furthermore, standard errors of interval boundary and peak maxima energies are close to the resolution of the 256-channel data sets (i.e., the higher resolution of the 2048-channel data does not improve overall spectral analysis).

All linear regressions and estimation error analyses were performed for both energy resolutions. Both data sets yield the same useful estimator segments. The R and estimation error values of the useful estimator segments vary less than 1% between the 2048- and 256-channel data sets. Therefore only the 256-channel results are presented in Table 4.

Grasty et al. (1985) analyzed airborne gamma-ray spectra collected with a 256-channel analyzer. They compared errors in concentration estimates for window sizes of 12, 48, 96, and 192 KeV, and found that Th and U errors from the 12 and 48 KeV wide-window analysis were reduced by up to 25% when compared to those resulting from the three-window method proposed by the IAEA (International Atomic Energy Agency, 1976). The 96- and 192-KeV window tests had a slightly higher error than the 12- and 48-KeV runs. The authors were in agreement with other studies of airborne spectra that 50 KeV wide windows were more than adequate to minimize concentration errors. As service companies, including Schlumberger, are moving towards acquisition of 256-channel data, the ODP should do the same. Our study shows that 2048-channel acquisition would only cause excessive data storage requirements, without adding quality to spectral analysis. Given the nature of the natural gamma-ray spectrum as resolved by scintillation detectors, an energy resolution of about 10 KeV (256 channels) is more than sufficient for estimation of K, U, and Th.

Standard Energy Windows

Many of our calculated energy interval boundaries conform well with intervals proposed by the IAEA (International Atomic Energy Agency, 1976) and used by Schlumberger Services (see Table 2 and Fig. 2 for energy intervals), but our analysis divides the spectrum further. Our intervals 6, 9, and 14, including the main peaks for K, U, and Th, respectively, cover practically the same intervals suggested by the IAEA for estimation of these elements. The five windows Schlumberger Services have been using for more than a decade closely correspond, respectively, to our intervals 0, intervals 1 through 4, intervals 5 and 6, intervals 7 through 10, and intervals 11 through 16.

Even though the method of Grasty et al. (1985) differs from our method, some results of their window optimization are comparable. In an attempt to improve U estimates, Grasty et al. (1985) examined two windows in addition to the three IAEA windows. One corresponds approximately to our interval 5, including the ^{214}Bi peak at 1120 KeV, and the other to our combined intervals 5 and 9. The authors concluded that errors in estimated U and K concentrations increased. This is consistent with our assessment that spectral segments other than P6 degrade the K estimate, and that interval 5 is not a useful estimator for U.

Grasty et al. (1985) also optimized positions for 10 adjacent, fixed windows between 0.77 and 2.83 MeV so that the uranium error was minimized. They found that estimates from using 10 selected windows was a good compromise between the three-window method and

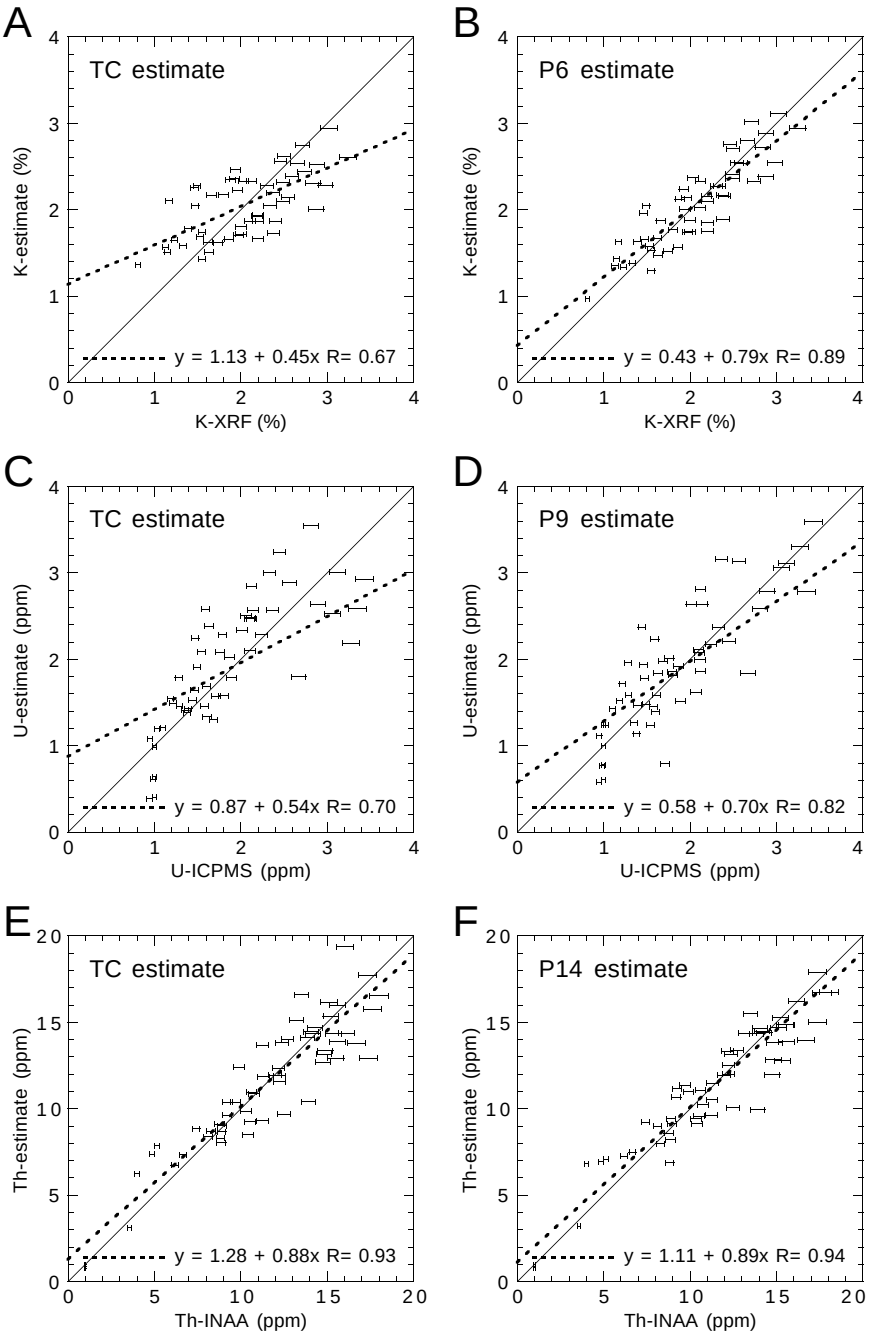

Figure 5. Reference concentrations vs. concentrations estimated from NGR counts. For each of the three elements K, U, and Th, estimates from total counts (**A**, **C**, **E**) and estimates from the best estimator spectral segment (**B**, **D**, **F**) are shown, illustrating the maximum improvement achieved by the spectral analysis presented here. Linear coefficients are for least squares regression (dashed line). Solid line is diagonal. Error bars are maximum analytical error of reference data (sum of absolute precision and accuracy in percent).

a more elaborate full-spectrum analysis, giving almost the same accuracy as estimates from full spectra with 12 KeV resolution. Our study identifies 11 potentially useful segments in seven energy intervals, with interval boundaries consistently different from the 10-window boundaries of Grasty et al. (1985). The discrepancy may be related to the difference between the strictly statistical, maximum-likelihood method used by Grasty et al. (1985) and our peak identification method, which ties interval boundaries to minima between peaks.

Our study suggests that for routine logging with the NGR (10- to 30-s counting time), total counts for U and Th estimates and interval 6 (or better, peak area P6) for K estimates is all that is needed. Nevertheless, it seems reasonable that the ODP core logger provide the capability of 256-channel acquisition and archiving. This ensures that calibrations and quality control can be performed later by any investigator's preferred method. If routine 256-channel spectra pose a data management problem (hundreds of megabytes every two months), acquisition and archiving of a set of three to ten fixed energy intervals (regions of interest) should also be considered for normal, routine core logging where counting time is insufficiently long to yield useful 256-channel spectra.

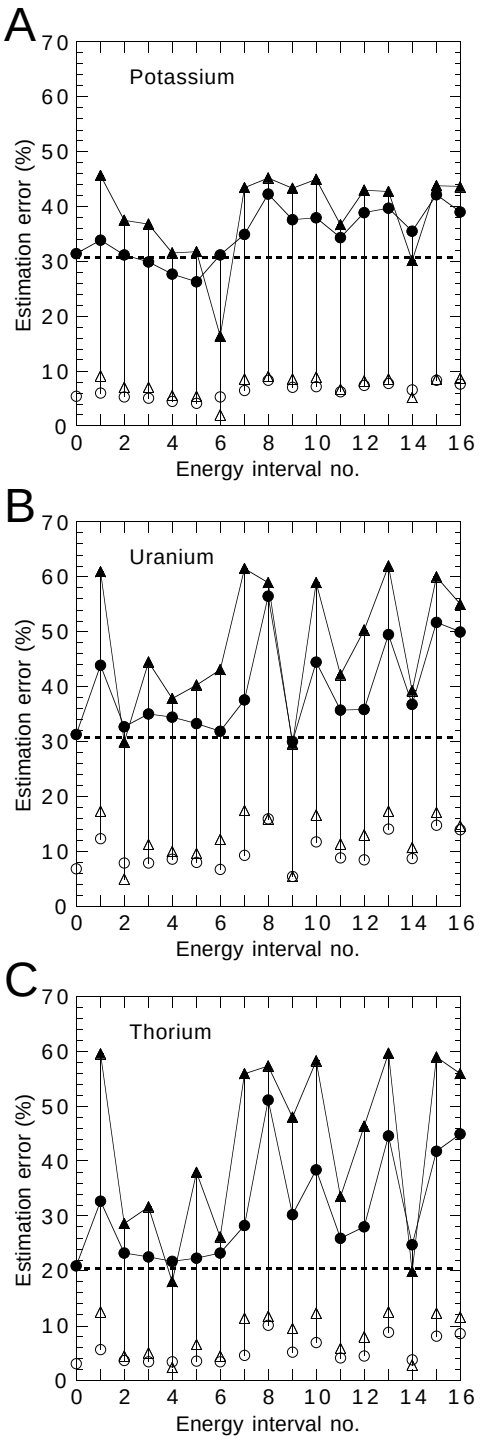

Figure 6. Estimation errors for spectral segments. **A.** Potassium. **B.** Uranium. **C.** Thorium. Triangles are values for peak areas and circles are values for background areas in any given energy interval. Deviation of estimated concentration from reference concentration, expressed as percentage of the reference concentration, is defined as percent deviation. Empty symbols are means of all percent deviations from 53 samples. Vertical lines are standard deviations of all percent deviations from 53 samples. Solid symbols represent the sum and therefore a conservative, maximum estimation error. This error includes analytical errors of reference data and the true estimation error may therefore be significantly smaller. Dashed lines are estimation errors using total counts as estimator. Only errors below that line indicate potentially useful estimator segments.

Eventually, standard reporting of elemental estimates could be provided using the best calibration and inversion method available. If the results of this study were to be used, integrated counts S_{P6} for peak area P6 would be computed according to our method, and elemental concentrations could be calculated using the following linear coefficients:

$$x'_K = 0.506 + 1.43S_{P6} \pm\left(16 + \frac{0.67\sqrt{S}}{S}100\right)\%$$

$$x'_U = 0.279 + 0.0762S_{TC} \pm\left(30 + \frac{0.67\sqrt{S}}{S}100\right)\%$$

$$x'_{Th} = 1.66 + 0.389_{TC} \pm\left(20 + \frac{0.67\sqrt{S}}{S}100\right)\%\ , \qquad (7)$$

Where all integrated counts S are normalized to counts per second (cps) and full-core measurement, S_{TC} is total count rate, x'_K is in wt%, x'_U and x'_{Th} are in ppm, and the error term includes our maximum estimation error and the counting (Poisson) error. The linear relationships with TC are dependent on the ratio of elemental concentrations contributing to TC. Our estimation error accounts at least for variations in these ratios represented by our reference data, and the relationships should hold fairly well for common rocks and sediments measured in the NGR system of ODP. More sophisticated calibration matrices will be developed and better estimates achieved once customized calibration standards are available.

Geological Application of Elemental Estimates

A detailed analyses and interpretation of K, U, and Th elemental data in their local geological context is best done in conjunction with other data, such as bulk and clay mineralogy, porosity, and other major and minor elemental data obtained from the same samples. Such an analysis is beyond the scope of this study, which focused on the potential use of the NGR device to obtain meaningful data from natural gamma-ray spectra. We therefore limit ourselves to a few general comments.

Well-logging services have established a vast number of concepts, algorithms, and programs to interpret K, U, and Th concentrations from NGR acquisition, along with other physical and chemical log parameters for different environments (see Serra, 1984, 1986, for an overview and references). Some of the concepts have also been criticized because they are often applied without consideration of additional, pertinent data, and with the lack of rigorous error estimates (Hurst, 1990). Some applications potentially useful for the Barbados accretionary wedge are estimation of clay volume and type, which exert a significant control on the structural evolution and fluid-flow paths, and leaching and precipitation of uranium as a direct consequence of fluid flow. Relative changes in the abundance of the three elements, together with other data, will allow testing of hypotheses in regard to the evolution of the décollement zone.

A quick look at our data shows that in Hole 948C, K, U, and Th decrease downhole at constant rates from 420 to 495 mbsf, the top of the décollement, from which their concentrations increase throughout the décollement (Fig. 3). Clay content increases downhole within the décollement from ~60 to 70 wt%, as estimated from shipboard X-ray diffraction analyses (Shipley, Ogawa, Blum, et al., 1995). K and Th, potential indicators of shaliness, both increase by about 100%, which means that a significant change in mineralogy must also occur at this level. Potential interpretations are a change in clay mineralogy (e.g., illite vs. smectite), or a change in concentration of certain heavy minerals. U increases only very slightly within the décollement. However, it continues to increase below the décollement and has its maximum between 520 and 530 mbsf. The U spikes are not entirely compatible with lithologic units described on Leg 156, and their position near the bottom of the décollement may suggest that leaching or precipitation is involved. However, such a hypothesis needs to be carefully tested with additional data and analyses.

Table 5. Comparison of estimation error and counting error at two different counting times.

			4 hr counting time (split-core)				20 s counting time (full-core)			
		Segment estimation error (%)	Segment average counts	Cumul. counts	Cumul. estimation error (%)	Cumul. counting error (%)	Segment average counts	Cumul. counts	Cumul. estimation error (%)	Cumul. counting error (%)
K	P6	16.3	7,792	7,792	16.3	0.76	22	22	16.3	14.50
	B5	26.3	6,653	14,445	20.9	0.56	18	40	20.9	10.65
	B4	27.7	8,952	23,397	23.5	0.44	25	65	23.5	8.37
	B3	29.9	8,548	31,945	25.2	0.38	24	89	25.2	7.16
	Total	30.1	172,263	172,263	30.1	0.16	479	479	30.1	3.08
U	P9	29.5	296	296	29.5	3.92	1	1	29.5	74.39
	P2	29.9	3,214	3,510	29.9	1.14	9	10	29.9	21.60
	B9	30.0	987	4,497	29.9	1.01	3	12	29.9	19.08
	B0	31.3	3,013	7,510	30.5	0.78	8	21	30.5	14.77
	B6	31.9	103,823	111,333	31.8	0.20	288	309	31.8	3.84
	Total	32.0	172,263	172,263	32.0	0.16	479	479	32.0	3.08
Th	P4	18.1	3,451	3,451	18.1	1.15	10	10	18.1	21.79
	P14	19.9	1,131	4,582	18.5	1.00	3	13	18.5	18.91
	Total	20.2	172,263	172,263	20.2	0.16	479	479	20.2	3.08

Notes: Cumul. = cumulative over the spectral segments (peak and background areas) listed for each element, except Total = total counts. Only spectral segments are listed, because spectral segments have decreased estimation errors when compared to total counts. Cumulative counting errors are based on cumulative counts. The 20 s counts were calculated by dividing the 4 hr counts by 360, which includes the factor of two correction for equivalent measurements.

From 520 mbsf downhole, concentration of all three elements fluctuates strongly, reflecting the interlayering of quite different sediment types. It will be possible to characterize the composition of each lithotype with the NGR and other elemental data to draw conclusions in regard to provenance and depositional process of the sequence.

Hole 949B is represented by scarce data because of low core recovery. We are able to observe spikes in U and Th concentrations at two or three levels that are probably related to thrust faults. A general increase in abundance of all three elements is associated with the décollement zone below 400 mbsf.

CONCLUSIONS

NGR spectra between 0.2 to 3.0 MeV are optimally resolved by 16 energy intervals divided into peak and background segments. Regression using five peak areas and six background areas gives better elemental estimates than regression using total counts of the entire spectrum. Potassium abundance should be estimated using the P6 peak area only, because other segments significantly increase the estimation error. Taking into account the error of counting statistics, it appears advantageous to estimate Th and U from total counts when low counting times are used. Lowest estimation errors from our analyses are 16% for K using peak area P6, 30% for U using P9, and 20% for Th using P4.

Acquisition of 2048-channel data is not warranted. In our experiment, we obtained more than sufficient spectral resolution using 256-channel binning, and the estimation error did not increase. ODP should implement 256-channel NGR data acquisition for their core logging system, which is becoming the standard in well logging and airborne survey as well.

ACKNOWLEDGMENTS

Reviews by Carlos Pirmez, Bill Bush, and Christian Bücker helped clarify the manuscript. This study was supported by USSSP award no. 156-20853b.

REFERENCES

Adams, J.A.S., and Gaspirini, P., 1970. Gamma ray spectrometry of rocks. *Meth. Geochem. Geophys.*, 10: Amsterdam (Elsevier).

Gladney, E.S., Jones, E.A., Nickell, E.J., and Roelandts, I., 1992. 1988 compilation of elemental concentration data for USGS AGV-1, GSP-1, and G-2. *Geostand. Newsl.*, 16:111–300.

Grasty, R.L., 1975. Uranium measurement by airborne gamma-ray spectrometry. *Geophysics*, 40:503–519.

Grasty, R.L., Glynn, J.E., and Grant, J.A., 1985. The analysis of multichannel airborne gamma ray spectra. *Geophysics*, 50:2611–2620.

Hoppie, B.W., Blum, P., and the Shipboard Scientific Party, 1994. Natural gamma-ray measurements on ODP cores: introduction to procedures with examples from Leg 150. *In* Mountain, G.S., Miller, K.G., Blum, P., et al., 1994. *Proc. ODP, Init. Repts.*, 150: College Station, TX (Ocean Drilling Program), 51–59.

Hurst, A., 1990. Natural gamma-ray spectrometry in hydrocarbon-bearing sandstones from the Norwegian Continental Shelf. *In* Hurst, A., Lovell, M.A., and Morton, A.C. (Eds.), *Geological Applications of Wireline Logs.* Geol. Soc. Spec. Publ. London, 48:211–222.

International Atomic Energy Agency, 1976. Radiometric reporting methods and calibration in uranium exploration. *Tech. Rep. Ser.- I. A. E. A*, 174.

Marett, G., Chevalier, P., Souhaite, P. and Suau, J., 1976. Shaly sand evaluation using gamma ray spectrometry, applied to the North Sea Jurassic. *SPWLA 17th Ann. Logging Symp.*, 1–20.

Mathis, G.L., Rutledge, D.R., and Ferguson, W.E., 1984. A spectral gamma ray (SGR) tool. *SPWLA 25th Ann. Logging Symp.*, 1–21.

Serra, O., 1984. *Fundamentals of Well-Log Interpretation* (Vol. 1): *The Acquisition of Logging Data*: Dev. Pet. Sci., 15A: Amsterdam (Elsevier).

————, 1986. *Fundamentals of Well-Log Interpretation* (Vol. 2): *The Interpretation of Logging Data:* Dev. Pet. Sci., 15B: Amsterdam (Elsevier).

Serra, O., Baldwin, J. and Quirein, J., 1980. Theory, interpretation and practical applications of natural gamma ray spectroscopy. *Trans. SPWLA 21st Annu. Logging Symp.*, 27:Q1–Q30.

Shipley, T.H., Ogawa, Y., Blum, P., et al., 1995. *Proc. ODP, Init. Repts.*, 156: College Station, TX (Ocean Drilling Program).

Till, R., 1974. *Statistical methods for earth sciences.* New York (John Wiley & Sons).

Date of initial receipt: 19 February 1996
Date of acceptance: 3 September 1996
Ms 156SR-024